



## Short Communication

## Development of a carbazole-based fluorescence probe for G-quadruplex DNA: The importance of side-group effect on binding specificity

Ming-Qi Wang\*, Gui-Ying Ren, Shuang Zhao, Guang-Chang Lian, Ting-Ting Chen, Yang Ci, Hong-Yao Li

School of Pharmacy, Jiangsu University, Zhenjiang 212013, PR China

## ARTICLE INFO

## Article history:

Received 15 September 2017

Received in revised form 26 March 2018

Accepted 30 March 2018

Available online 05 April 2018

## Keywords:

G-quadruplex DNA

Fluorescent probe

Carbazole

Side group

## ABSTRACT

G-quadruplex DNAs are highly prevalent in the human genome and involved in many important biological processes. However, many aspects of their biological mechanism and significance still need to be elucidated. Therefore, the development of fluorescent probes for G-quadruplex detection is important for the basic research. We report here on the development of small molecular dyes designed on the basis of carbazole scaffold by introducing styrene-like substituents at its 9-position, for the purpose of G-quadruplex recognition. Results revealed that the side group on the carbazole scaffold was very important for their ability to selectively recognize G-quadruplex DNA structures. **1a** with the pyridine side group displayed excellent fluorescence signal turn-on property for the specific discrimination of G-quadruplex DNAs against other nucleic acids. The characteristics of **1a** were further investigated with UV-vis spectrophotometry, fluorescence, circular dichroism, FID assay and molecular docking to validate the selectivity, sensitivity and detailed binding mode toward G-quadruplex DNAs.

© 2018 Elsevier B.V. All rights reserved.

## 1. Introduction

Guanine-rich DNA sequences can fold into four-stranded secondary structures known as DNA G-quadruplexes, which were different from the regular double helix [1–4]. Based on mutual strand orientation, they can adopt a wide range of topologies, i.e. parallel, antiparallel, hybrid of parallel and antiparallel [2]. DNA G-quadruplexes predominantly exist in the chromosomal telomeric sequences and the promoter regions of genes, such as c-myc, ckit, HRAS, VEGF [5–7]. In recently years, DNA G-quadruplex structures have received immense attention because their unique structural features are believed to be able to provide biological significance in transcriptional regulation, DNA replication, telomere maintenance and antitumor chemotherapy [8–12]. At the same time, the research of DNA G-quadruplexes is in the center stage and many aspects of their biological mechanism and significance still need to be elucidated.

Given the importance of DNA G-quadruplexes, the ever-increasing interest has promoted the development of the rapid and simple approaches for G-quadruplex detection. Fluorescence probes provide a powerful and direct means for studying the folding, function, and localization of biological macromolecules in vitro and in vivo [13]. Thus, fluorescence probes that capable of reporting DNA G-quadruplex structures are extremely attractive [14–16]. Recently, some small molecular based fluorescence probes have been identified for analysis of DNA G-

quadruplex, such as thioflavin T [17], naphthalene diimide [18], thiazole orange derivatives [19], triphenylamine [20], quinolinium [21], tetra-arylimidazole [22]. Among the reported studies, carbazole is one of the most frequently applied scaffolds for DNA G-quadruplex probe modification probably due to its merit property in pharmacological activities. Successful examples include BMVC [23], TO-CZ [24], BPBC [25] and 9E PBIC [26]. Interestingly, the cationic charge groups at 3 and 6 positions of carbazole scaffold play essential roles in the enhancing their binding potency on G-quadruplex DNA. For example, the molecular 3,6 bis(1 methyl 4 vinylpyridinium)carbazole diiodide (BMVC) for recognizing specific quadruplex structures has attracted much attention [23]. However, BMVC has similar binding affinities for G-quadruplex and duplex DNA. Seeking new probes that possessing better selectivity is important for further applications. With respect to the literatures, how a small cationic charge pendant substituent applied to the 9-position of carbazole core can induce selectivity fluorescence signal toward G-quadruplex is unclear and has not been discussed. In the present study, we reported two new fluorescence dyes, designed on the basis of carbazole scaffold by introducing styrene-like substituents at its 9-position, for the purpose of investigating the influence of side groups on developing the effective fluorescence probes for G-quadruplex recognition. **1a** was designed by linking a cationic pyridinium unit to the carbazole core via a vinyl group, whereas **1b** possesses a cationic quinolinium compared to **1a**. The characteristics of the dyes toward DNA G-quadruplexes were investigated through both experimental and modeling studies. Both of them are able to bind with G-quadruplex DNAs, and excellent fluorescence discrimination with

\* Corresponding author.

E-mail address: [wmq3415@163.com](mailto:wmq3415@163.com). (M.-Q. Wang).

non-G-quadruplex and G-quadruplex structures is found to be determined by **1a**. In addition, the optical properties and the binding mechanism of **1a** were further investigated and discussed.

## 2. Experimental Sections

### 2.1. Materials

All commercially available chemicals used for synthesis were reagent grade and used without further purification. The  $^1\text{H}$  NMR and  $^{13}\text{C}$  NMR spectra measured on a Bruker AM400 NMR spectrometer and the  $\delta$  scale in ppm referenced to residual solvent peaks or internal tetramethylsilane (TMS). Mass spectra (MS) were recorded on a Shimadzu LCMS-2010A instrument with an ESI detector. Oligonucleotides (HPLC purified) were purchased from Sangon Biotechnology Co. Ltd. (Shanghai, China) and the sequences were listed in Table S1. Oligonucleotides were dissolved in 10 mM Tris-HCl buffer (pH 7.4, containing 60 mM KCl). Prior to use, all oligonucleotides were pre-treated by heating at 95 °C for 5 min, followed by gradual cooling to room temperature and kept at this temperature for 0.5 h. The ct-DNA, purchased from Sigma Aldrich, was directly dissolved in water at a concentration of 1 mg/mL. Its concentration was determined according to absorption intensity at 260 nm with a molar extinction coefficient value of 6600. Stock solutions of 2 (5 mM) were prepared in DMSO and stored at 4 °C.

### 2.2. Synthesis and Characterization

#### 2.2.1. 2 [4 (9H Carbazol 9 yl)styryl] 1 methylpyridinium Iodide **1a**

A solution of intermediate 4 (9H carbazol 9 yl)benzaldehyde **3** (0.27 g, 1.0 mmol), 1 methyl 2 picolinium iodide (0.2 g, 0.85 mmol) and 5 drops piperidine in anhydrous ethanol (50 mL) was refluxed for 12 h under nitrogen with stirring. After cooling to room temperature, a precipitate was formed during the process of reaction. The reaction mixture was filtered, and washed thoroughly with anhydrous ethanol. The residue was purified by column chromatography on silica gel eluting with  $\text{CH}_2\text{Cl}_2/\text{CH}_3\text{OH}$  (10:1, v/v) to afford **1a** (0.24 g, 57.9%) as a yellow solid.  $^1\text{H}$  NMR (400 MHz, DMSO  $d_6$ )  $\delta$ : 8.84–8.82 (m, 2H), 8.53 (d,  $J = 7.68$  Hz, 1H), 8.43 (t,  $J = 7.76$  Hz, 1H), 8.31 (d,  $J = 7.64$  Hz, 1H), 8.15–8.11 (br, 1H), 7.91–7.89 (m, 1H), 7.81–7.77 (m, 1H), 7.69–7.65 (m, 2H), 7.63–7.59 (br, 3H), 7.56–7.52 (m, 1H), 7.47–7.43 (m, 1H), 7.40–7.38 (br, 1H), 7.35–7.31 (br, 2H), 4.38 (s, 3H);  $^{13}\text{C}$  NMR (100 MHz, DMSO  $d_6$ )  $\delta$ : 150.30, 146.22, 144.60, 144.32, 142.01, 141.38, 136.73, 130.80, 128.63, 127.77, 127.20, 121.99, 121.35, 115.05, 110.62, 46.67; LC-MS: (positive mode,  $m/z$ ) calculated 361.1699, found 361.1687 for  $[\text{M}-\text{I}]^+$ .

#### 2.2.2. 2 [4 (9H Carbazol 9 yl)styryl] 1 methylquinolinium Iodide **1b**

Following the general procedure for **1a**, the product **2a** was obtained as a brown solid (0.32, 53.8%).  $^1\text{H}$  NMR (400 MHz, DMSO  $d_6$ )  $\delta$ : 8.93–8.91 (m, 2H), 8.58 (d,  $J = 9.12$  Hz, 1H), 8.46 (t,  $J = 8.8$  Hz, 2H), 8.32 (d,  $J = 7.6$  Hz, 1H), 8.23 (d,  $J = 8.0$  Hz, 1H), 8.08–8.04 (m, 1H), 8.00–7.98 (m, 1H), 7.94–7.90 (m, 1H), 7.84 (t,  $J = 7.56$  Hz, 1H), 7.72–7.69 (m, 2H), 7.63–7.56 (m, 3H), 7.49–7.45 (m, 1H), 7.40–7.33 (m, 3H), 4.55 (s, 3H);  $^{13}\text{C}$  NMR (100 MHz, DMSO  $d_6$ )  $\delta$ : 156.70, 148.96, 143.77, 142.44, 141.39, 139.57, 136.58, 135.02, 130.81, 130.35, 129.05, 128.95, 128.72, 127.84, 127.75, 127.63, 127.18, 123.91, 123.06, 122.69, 121.52, 121.35, 121.14, 119.56, 116.64, 110.70, 110.67, 41.92. LC-MS: (positive mode,  $m/z$ ) calculated 411.1856, found 411.1848 for  $[\text{M}-\text{I}]^+$ .

### 2.3. Measurements and Methodology

#### 2.3.1. Fluorimetric Titrations

Fluorescence spectra were measured on a Shimadzu RF-5301PCS spectrofluorophotometer in a 10 mm quartz cell at room temperature. The concentration of **1a/1b** was fixed at 2  $\mu\text{M}$  in buffer, to which the DNA solution was added step by step. Dye-DNA solution was incubated

for 1 min before fluorescence spectra recorded. The volume of the dye was 2.5 mL and the changes in the dye concentration caused by dilution at the end of each titration were negligible. For **1a** and **1b**, the fluorescence measurement was obtained at an excitation wavelength of 404 and 480 nm, respectively. The data from the fluorimetric titrations were analyzed according to the independent-site model by nonlinear fitting to equation [27], in which  $n$  is the putative number of **1a** molecules binding to a given DNA matrix,  $Q$  is the fluorescence enhancement upon saturation,  $A = 1/[K_a C_{\text{dye}}]$ . The parameters  $Q$  and  $A$  were found by Levenberg-Marquardt fitting routine in Origin 8.5 software, whereas  $n$  was varied to obtain a better fit.

$$\frac{F}{F_0} = 1 + \frac{Q-1}{2} \left[ A + 1 + x - \sqrt{(A + 1 + x)^2 - 4x} \right]$$

#### 2.3.2. UV-vis Titrations

The UV-vis spectra were recorded on an UV-2550 spectrophotometer using a 1 cm path length quartz cuvette at room temperature. For the titration experiments, small aliquots of a stock solution of the DNAs were added to the solution containing **1a** at a fixed concentration (8  $\mu\text{M}$ ) in aqueous buffer (10 mM Tris-HCl, pH 7.4, 60 mM KCl). After each DNA addition, the solution was incubated for 1 min before absorption spectra recorded.

#### 2.3.3. Fluorescence Intercalator Displacement (FID) Assay

The FID experiment was carried out with thiazole orange (TO) as a fluorescence probe and the protocol was similar to those described elsewhere [20]. The concentrations of TO and G-quadruplex 22AG were set at 0.5 and 0.1  $\mu\text{M}$ , respectively. **1a** was added until no change was observed in the fluorescence intensity indicating the binding saturation has been achieved. The fluorescence spectra were measured using excitation wavelength at 504 nm and the emission range was set between 515 and 700 nm.

#### 2.3.4. Circular Dichroism (CD)

The concentration of G-quadruplex used for measurement was 4  $\mu\text{M}$  in 10 mM Tris-HCl buffer, pH 7.4 in the presence of 60 mM KCl and the concentration of **1a** was 1–2 folds. CD spectra (230–400 nm) were performed on a JASCO-J815 circular dichroism spectrophotometer using a 10 mm path length quartz cuvette. The scanning speed of the instrument was set to 400 nm  $\text{min}^{-1}$ . Final analysis of the data was carried out using Origin 8.5.

#### 2.3.5. KI Quenching

KI quenching was carried out in the presence and absence of 22AG. A 2.5 mL reaction vessel was prepared containing **1a** (2  $\mu\text{M}$ ) and 10 mM Tris-HCl (pH 7.4, containing 60 mM KCl). Emission fluorescence of mixture was acquired after adding increasing concentration of KI (with the concentration range of from 0 to 1 M) which is a known quencher. The fluorescence quenching spectra were recorded and were fitted by using the Stern-Volmer equation.

#### 2.3.6. Molecular Docking

Molecular docking calculations were performed using the Autodock Vina software, which has been reported to be of high accuracy of prediction [28]. The crystal structure (PDB code: 1KF1, resolution: 2.10 Å) and the NMR structure (PDB code: 143D) of G4 DNA were downloaded from RCSB Protein Data Bank. The redundant solvent molecules and ions were removed from the crystal structure while the first conformation was retained from the NMR structure. Docked poses were visualised by using UCSF Chimera.

### 3. Results and Discussion

#### 3.1. Synthesis of New Fluorescence Dyes

As shown in Scheme 1, intermediate **3** (4-(9H-carbazol-9-yl)benzaldehyde) was obtained by the reaction of **2** (*N*-phenylcarbazol) with DMF/POCl<sub>3</sub> (Vilsmeier reagent). The targeted fluorescence dyes **1a** and **1b** with different styryl substituents were synthesized by the reaction of **3** with *N*-methylated aromatic groups including 1-methyl-2-picoliniumiodide (**1a**) and 1-methyl-2-quinoliniumiodide (**1b**). The structures of these two new dyes were characterized by <sup>1</sup>H NMR, <sup>13</sup>C NMR and MS (see the Supplementary information).

#### 3.2. Selectivity Study of New Dyes Toward G-quadruplex DNAs Against Other Nucleic Acids

The selectivity of these new dyes to G-quadruplex DNAs was first investigated and evaluated by using the fluorescence spectra of the dyes in the presence of different DNA forms including G-quadruplexes, single- and double-stranded DNAs and the protein BSA. As shown in Fig. 1, the enhanced fluorescence intensity of **1a** was found to be remarkable upon binding with different G-quadruplex DNAs (parallel, anti-parallel and hybrid-type) at saturated concentration, while single- and double-stranded DNAs and the protein BSA showed negligible fluorescence enhancement, suggesting that **1a** could discriminate of G-quadruplexes from single-, double-stranded DNAs and BSA. In contrast, under the same experimental conditions, although **1b** responded to most of these DNAs and BSA, the enhanced intensity gave poor selectivity. These results validate the importance of side group of carbazole scaffold in achieving effective fluorescence probing of G-quadruplexes. Generally, **1a** with the pyridine side group has better performance than **1b** with the quinoline group for utilizing as a G-quadruplex selective fluorescent probe in bioassays. As a result, **1a** was chosen for further detailed studies.

#### 3.3. Fluorescence Properties of **1a** With DNA Forms

The detail fluorescence properties of **1a** with the DNA forms were studied by using fluorescence titration assay. As shown in Fig. 2A, **1a** alone in buffer displayed weak emission with a maximum wavelength at approximately 545 nm, which was remarkably enhanced by the

addition of telomeric G-quadruplex DNA 22AG. This turn-on fluorescence was also observed when **1a** was treated with the G-quadruplexes Ckit1, CM22, HRAS, Htg-21, C-myc, G3T3, Hras-2 and Ckit3. Almost no changes in the fluorescence spectra were observed when other oligonucleotides including single-stranded DNA (ss26), duplex DNA (ds26, ctDNA, Polyd(A-T)<sub>9</sub> and Polyd(G-C)<sub>9</sub>) were added (Fig. S1). These results suggest that **1a** exhibits a high selective fluorescence response toward G-quadruplex DNAs.

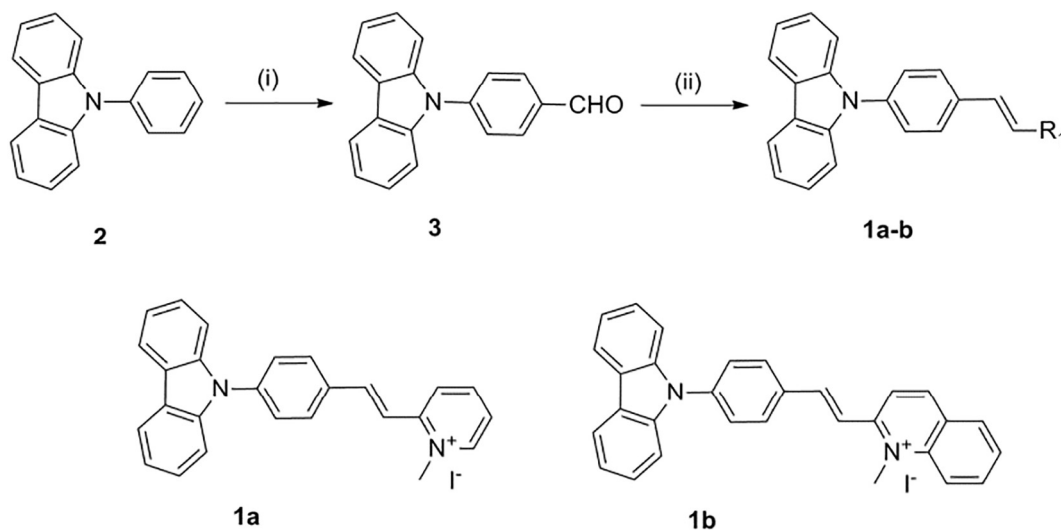
To ascertain the selective turn-on fluorescent signal is due to the specific binding of **1a** with G-quadruplex DNA structure, a competitive titration was conducted in the presence of a large excess of a duplex DNA (ctDNA, 50 μM) with 22AG G-quadruplex (Fig. 2B). At the high concentration of ctDNA, a weak background fluorescent signal of **1a** was observed. The addition of 22AG led to a significant enhancement of the fluorescence intensity, although the fluorescence of **1a** was somewhat affected by the presence of duplex DNA. The results revealed that **1a** possessed excellent specificity for G-quadruplex sensing in the competitive biological environment.

#### 3.4. Time-dependent Response

The response time of the probe was a key parameter for the biological application. We then proceeded to study the time-dependent response characteristic of the probe **1a** in the presence of 22AG was performed by using fluorescence spectra. As shown in Fig. 3, once 22AG was added, the fluorescence intensity of **1a** exhibited a sharp increase and reached the maximum within 10 s, meaning that the binding performance between **1a** and 22AG could be accomplished within 10 s at room temperature.

#### 3.5. UV-vis Absorption Spectroscopy

The ability of **1a** to interact with G-quadruplex DNA was also studied by spectrophotometric titration experiments. In aqueous buffer solution, **1a** shows a wide absorption band with a λ<sub>max</sub> at 402 nm. Fig. 4 shows that the maximum absorption wavelength of the **1a** in the **1a**-22AG system has very slight shift in λ<sub>max</sub> but its absorbance decreases significantly as compared with the free **1a** system. The similar changes in the spectral profiles of other G-quadruplex DNAs during titrations were shown in Fig. S2. It is a generally accepted concept that unimportant (or small) shift in maximum wavelength of absorption is the most



<sup>a</sup>Reagents and conditions: (i) DMF, POCl<sub>3</sub>, 80 °C, 15 h; (ii) reaction with N-methylated aromatic groups, piperidine, 80 °C, 12 h

Scheme 1. Synthesis route to **1a–b** and their molecular structures<sup>a</sup>.

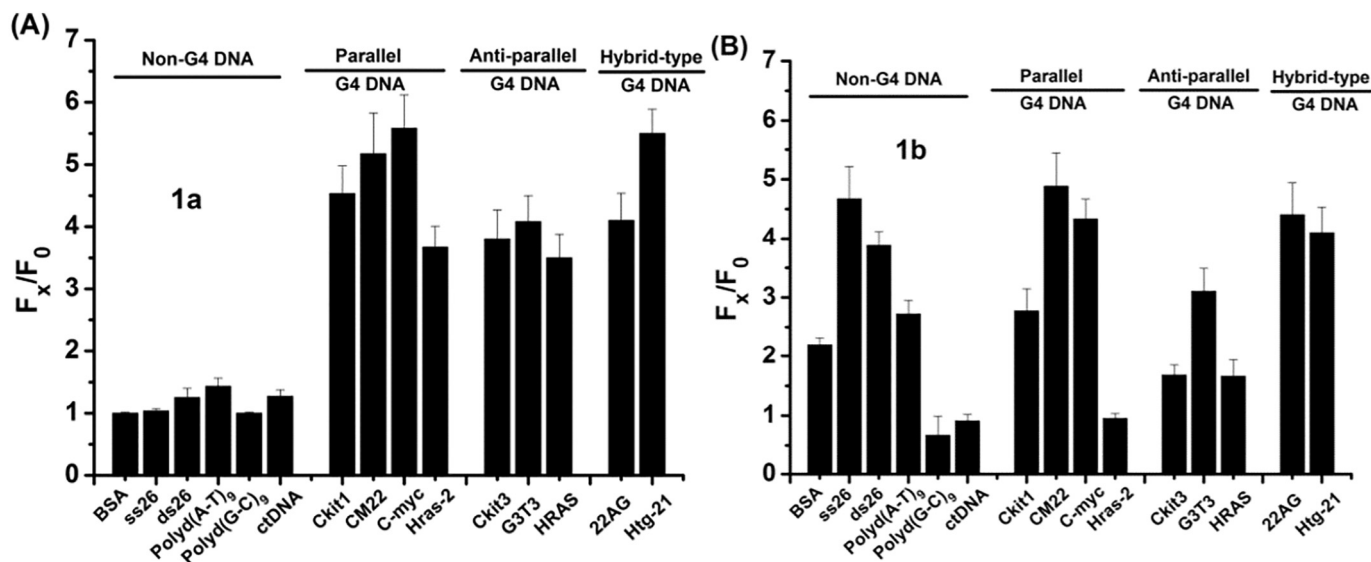


Fig. 1. Comparison of enhancement of emission intensity of **1a** and **1b** with BSA; single-, and double-stranded DNAs; G-quadruplexes DNAs. The concentration of the dyes was  $2 \mu\text{M}$  in 10 mM Tris-HCl buffer (pH 7.4) containing 60 mM KCl.

possible outcome of groove binding [29]. Thus, the recorded spectra indicated the binding between **1a** and G-quadruplex DNA was in the mode of groove binding rather than that of intercalation binding [30].

### 3.6. Binding Affinities and the Detection Limits (LOD) of **1a** With G-quadruplex DNAs

The binding properties of **1a** with G-quadruplex DNAs were also studied by fluorescence titrations. To estimate the binding constant ( $K_b$ ) and stoichiometry ( $n$ ) of **1a** to G-quadruplex DNA, the fluorescence titration curve was fitted to an independent-site model (see Experimental sections, Fig. S3) and the results were further confirmed by Job plot experiments (Fig. S4). The results presented in Table 1 revealed several regularities: 1) **1a** exhibited higher binding affinity to anti-parallel G-quadruplex DNAs (Ckit3, HRAS and G3 T3) and lower affinity to parallel (CM22, C-myc, Hras-2, Ckit1) and hybrid-type (22AG, Htg-21) G-quadruplex DNAs; 2) **1a** showed different binding stoichiometries to the tested G-quadruplex DNAs; 3) The binding affinities and fluorescence enhancements are not directly correlated, may due to the different microenvironments in the binding sites, which avoid the non-radiative relaxation process to different extents.

Encouraged by the fluorescence emission enhancement of **1a** with G-quadruplexes, we then investigated the detection limits (LOD) associated with using **1a** to G-quadruplexes in solution. The LOD values were calculated according to the equation  $3s/k$  [31]. The  $s$  value represents the standard deviation for multiple measurements of blank solution. The  $k$  value is the slope derived from the linear range of the **1a** fluorescence titration curve with different G-quadruplexes. The linear ranges of the fluorescence titration curves for **1a** with most of G-quadruplex DNAs ranged from 0.1 to  $1.0 \mu\text{M}$ . Thus, the corresponding values of the LODs were shown in Table 1 and (Fig. S5). Clearly, the LODs of **1a** for different G-quadruplexes in solution were below  $1 \mu\text{M}$ , which meant it was able to detect G-quadruplex DNAs in the micromolar range.

### 3.7. Effect of Potassium Ionic Strengths of G-quadruplex DNA on the Interactions With **1a**

G-quadruplex structures are inherently stabilized by the presence of alkali-metal cations which coordinated to O6 atoms of guanines in the quartet [9]. In order to study the effect of buffer cationic strength on this dye **1a** binding to G-quadruplex DNA, fluorescence titrations were

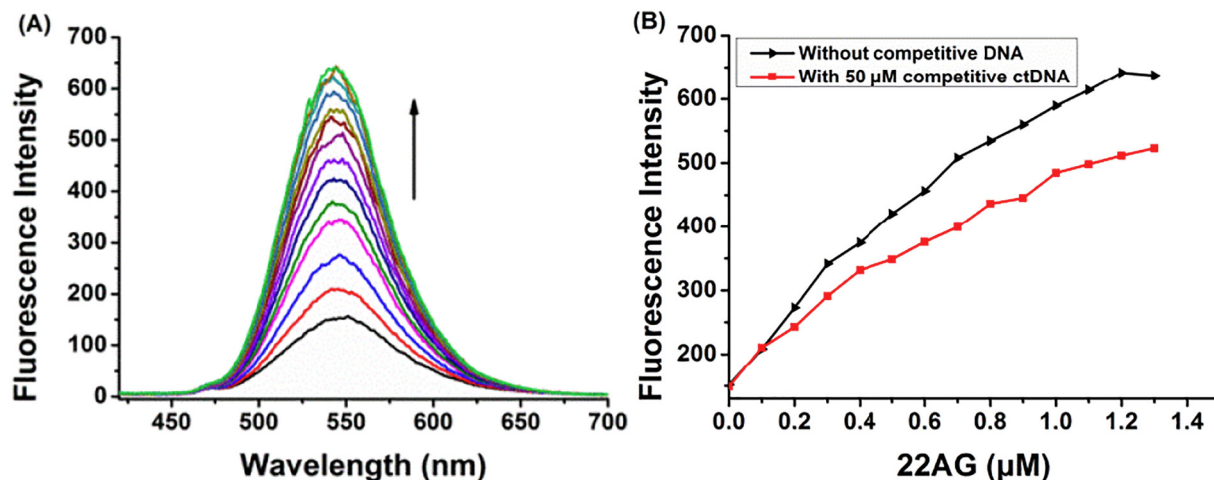


Fig. 2. (A) Fluorescence titration of  $2 \mu\text{M}$  **1a** with stepwise addition of the G-quadruplex DNA 22AG (0– $1.4 \mu\text{M}$ ) in 10 mM Tris-HCl buffer (pH 7.4) containing 60 mM KCl. (B) Fluorescence titration of  $2 \mu\text{M}$  **1a** with stepwise addition of the G-quadruplex DNA 22AG in the presence/absence of  $50 \mu\text{M}$  ctDNA in 10 mM Tris-HCl buffer (pH 7.4) containing 60 mM KCl.

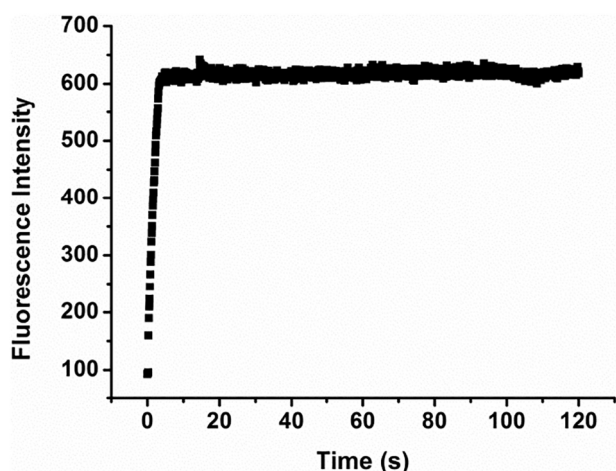


Fig. 3. The fluorescence intensity at 545 nm of **1a** (2  $\mu$ M) in the presence of 22AG (2  $\mu$ M).

carried out in different Tris-HCl buffer with variation in  $K^+$  concentrations (0–100 mM). Result emphasized that the value of enhancement in the fluorescence intensity of **1a** with 22AG was increased with increasing of buffer salt concentration, with maximal value occurring near 10 mM (Fig. 5). Above this concentration, however, it displayed a slight decrease. Perhaps because  $K^+$  ions preferentially stabilized the G-quadruplex with folding structures and only a low concentration of  $K^+$  ions is required for the structural stabilization. In the case of higher concentration of  $K^+$  ions, it demonstrates that  $K^+$  ions occupy the available binding sites on G-quadruplex surface and reduces the possibility for ligand to bind exterior of G-quadruplex [32]. The positively charged side group would enhance electrostatic interaction strength with the negatively charged DNA phosphate backbone. The dependence of the fluorescence enhancements on the ionic strength of the buffer indicates that the electrostatic interactions play an important role in the binding process.

### 3.8. Effect of **1a** on the Topologies of G-quadruplexes

To understand the effect of the dye on the topologies of G-quadruplexes, we deployed circular dichroism (CD) spectroscopy to monitor the formation of the G-quadruplex structure in the absence and presence of this dye. As shown in Fig. 6, the parallel G-quadruplex CM22 exhibited a characteristic positive peak at  $\sim$ 263 nm and a negative peak at  $\sim$ 242 nm. The anti-parallel G-quadruplex HRAS had a positive

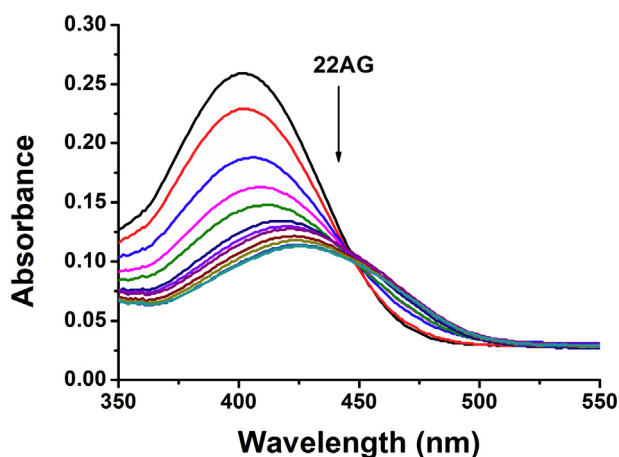


Fig. 4. Spectrophotometric titration of **1a** with 22AG in Tris-HCl buffer (10 mM, pH 7.4) containing 60 mM KCl. Conditions: [**1a**] = 8  $\mu$ M; [22AG] = 0–2.2  $\mu$ M. Arrows indicate the change in absorbance upon increasing the 22AG concentrations.

Table 1

Apparent binding constants ( $K_a$ ), binding stoichiometry ( $n$ ) and the detection limits (LOD) of **1a** to different G-quadruplex DNAs, determined from fluorimetric titrations. <sup>[a]</sup>Experimental conditions: **1a** = [2  $\mu$ M] in 10 mM Tris-HCl buffer (pH 7.4) containing 60 mM KCl; <sup>[b]</sup>Linear detection range.

G-quadruplex DNA <sup>[a]</sup>	Stoichiometry ( <b>1a</b> :DNA)	$K_a$ [ $10^6$ M <sup>-1</sup> ]	Lrd ( $\mu$ M)	LOD ( $\mu$ M)
22AG	3:1	0.33	0.1–0.7	0.11
CM22	1:1	1.45	0.1–0.4	0.065
C-myc	3:1	0.36	0.2–0.6	0.11
Ckit1	3:1	0.96	0.2–0.7	0.24
Ckit3	3:1	2.43	0.1–0.6	0.22
Htg-21	3:1	0.33	0.1–1.0	0.32
HRAS	3:1	6.58	0.2–0.6	0.24
G3 T3	4:1	3.88	0.1–0.4	0.10
Hras-2	1:1	0.28	0.1–1.0	0.27

peak at  $\sim$ 290 nm and a negative peak at  $\sim$ 255 nm. The telemetric hybrid-type G-quadruplex 22AG showed a strong positive peak at  $\sim$ 290 nm, a minor shoulder positive peak at  $\sim$ 270 nm and a negative peak at  $\sim$ 235 nm [33]. The addition of **1a** to these three G-quadruplexes had negligible impacts on the characteristic CD peaks, indicating that this dye can sense G-quadruplexes without affecting the G-quadruplex topologies.

### 3.9. Binding Mode Studies

The main binding modes of ligands with G-quadruplexes are end-stacking and grooves binding. To obtain the details on the interactions of **1a** with G-quadruplexes, an indirect fluorescent intercalator displacement (FID) assay by using thiazole orange (TO) was performed [34]. This method is based on the competitive displacement of fluorescence probe TO/G-quadruplex complex. TO is considered to bind G-quadruplex DNA mainly by an end-stacking mode and it consequently exhibits high fluorescence intensity ( $\sim$ 500- to 3000-fold). Dyes having the same binding site will compete with TO for G-quadruplex binding, resulting in the large decrease of the emission. As shown in Fig. 7A and B, in the presence of large (20 equiv) excess of **1a**, partial displacement of TO was detected and the 50% threshold was not reached. Since TO should be easier to displace by an end-stacking dye, this partial displacement may due to the groove binding mode between **1a** and G-quadruplex 22AG [35]. For comparison, **1b** with a quinolinium side chain was also studied. FID experiment of **1b** showed that fluorescence emission of TO was gradually reduced and almost completely quenched (Fig. S6). Therefore, one can conclude that **1b** exerted similar effect on

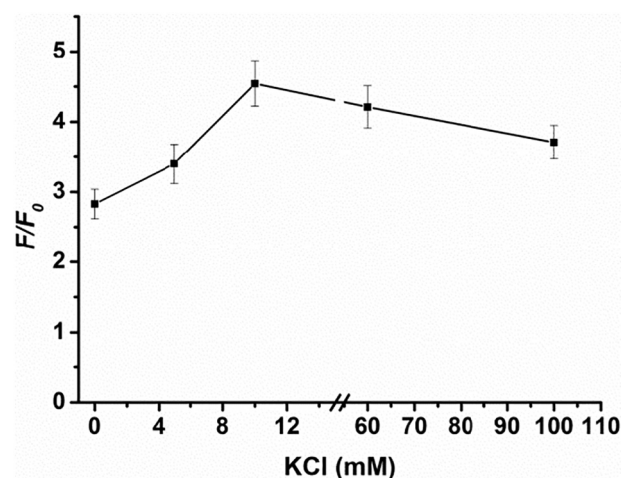


Fig. 5. Fluorescence enhancements of **1a** (2  $\mu$ M) at 545 nm with 22AG (1  $\mu$ M) in 10 mM Tris-HCl, pH 7.4, containing 0–100 mM KCl.

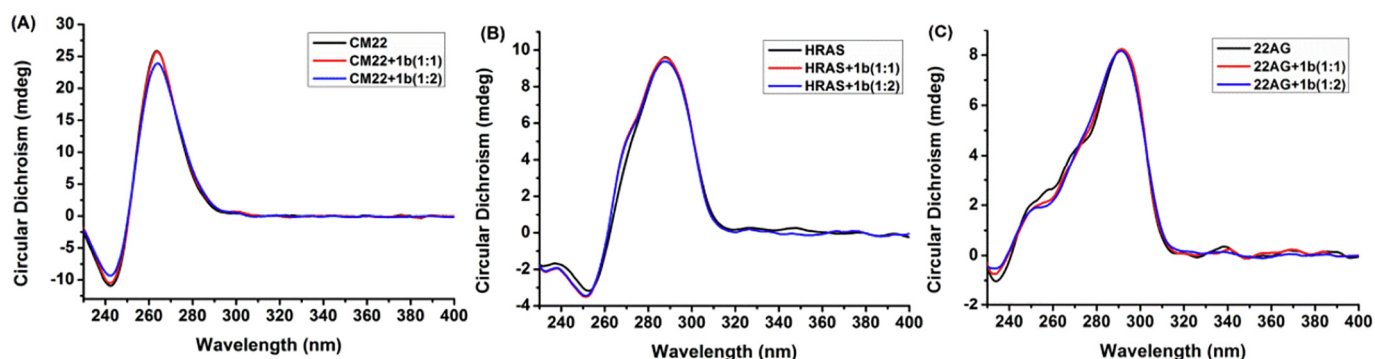


Fig. 6. CD spectra of 4  $\mu$ M G-quadruplex-forming oligonucleotides CM22 (A), HRAS (B), and 22AG (C) in 10 mM Tris-HCl buffer, 60 mM KCl, pH 7.4 with and without **1a**.

the TO, consisting in gradual release of TO from G-quadruplex structure. In general, this may be caused the quinolinium moiety may interact with G-quartet plane by  $\pi$ - $\pi$  stacking binding as previous reported [36]. From the FID experiments, in fact, different side group conjugating with the same scaffold can generate distinct G-quadruplex binding properties. Although the majority of dyes reported so far recognize G-quadruplexes by end-stacking binding mode. The groove binding may be the more promising binding mode, which is favorable for the

enhancement of selectivity. G-quadruplex topologies endow grooves with specific dimensions and accessibilities, which are different from various other structures. In order to further confirm the binding mode of **1a** to G-quadruplex DNA, its fluorescence quenching in the absence and presence of 22AG were studied by using a well-known quencher (potassium iodide). As reported in many studies, fluorescence intensity of an intercalating small molecule is well protected from being quenched as the approach of quencher e.g. iodide toward the

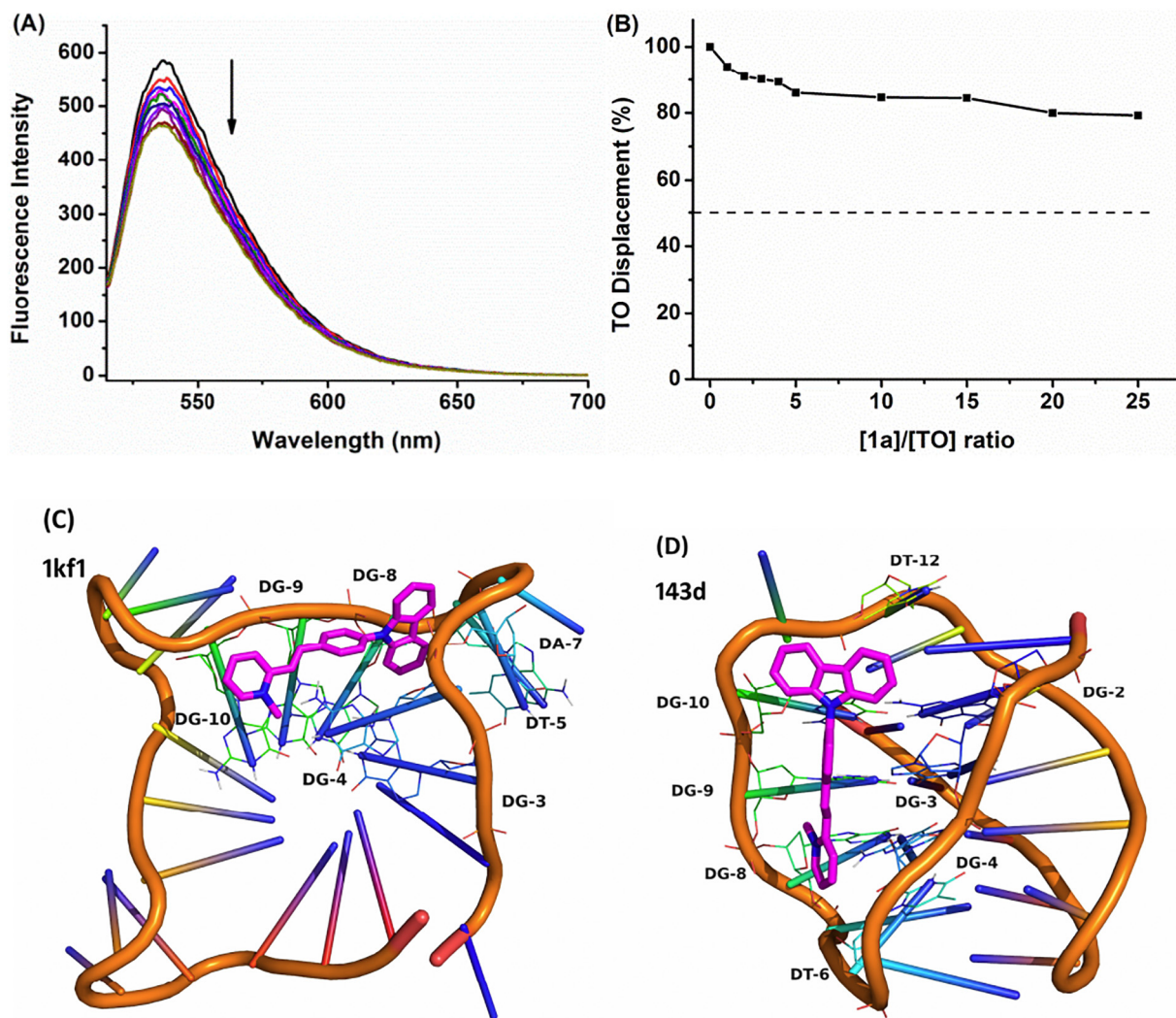


Fig. 7. (A) Fluorescence displacement of TO bound G-quadruplex 22AG by **1a** in 10 mM Tris-HCl buffer (pH 7.4, containing 60 mM KCl). Arrow shows the intensity changes upon increasing the concentration of **1a**. (B) Plot of TO displacement vs. ratio of **1a**/TO. (C) Molecular modeling for **1a** and parallel G-quadruplex 1kf1. (D) Molecular modeling for **1a** and anti-parallel G-quadruplex 143d.

fluorophore is restricted. However, groove binding affords little shield for the bounded molecule, so the fluorophore is exposed to the external environment and iodide anions can quench their fluorescence without difficulty even in the presence of DNA [37]. The obtained data were plotted according to the Stern-Volmer equation (Fig. S7) [38]. The values of  $K_{sv}$  of **1a** by  $I^-$  ion in the absence and presence of 22AG were calculated to be  $1.51 \text{ M}^{-1}$  and  $1.66 \text{ M}^{-1}$ , respectively. The  $K_{sv}$  value was higher than the quenching of **1a** by KI in the absence of 22AG and these findings are good proof of groove binding mode.

To gain further insight into the interactions of **1a** and G-quadruplexes, molecular docking studies were carried out by using AutoDock Vina modeling tool. The anti-parallel basket NMR G-quadruplex structure (PDB 143D) and a parallel-type crystal G-quadruplex structure (PDB 1KF1) were used as the templates for the docking studies. As displayed in Fig. 7C and D, the docking studies suggested that **1a** bound to these two G-quadruplexes in the groove region. The side group provided steric hindrance, and the molecule was non-planar and inserted into shallow groove of G-quadruplex DNA. Moreover, the modeling study revealed that **1a** bound to the anti-parallel G-quadruplex and parallel G-quadruplex with a calculated binding energy of  $-7.2$  and  $-8.2$  kcal/mol, respectively. Therefore, **1a** exhibited a superior binding energy to anti-parallel G-quadruplex to that of parallel G-quadruplex. This finding was consistent with the trend for binding constants of the G-quadruplexes as observed in the fluorescence titration assay.

#### 4. Conclusions

In conclusion, we have designed and investigated the specific G-quadruplex recognition ability of carbazole derivatives with different styrene-like substituents. To this end, two new dyes **1a** and **1b** were synthesized and structurally characterized. Result showed that different side group conjugating with the same scaffold can generate distinct G-quadruplex binding properties. **1a** with pyridine side group can discriminate G-quadruplex from duplex and single-stranded DNA based on its significant fluorescence enhancement in the presence of G-quadruplexes, while **1b** with quinolinium group gave poor selectivity. The result hints that side group plays an important role in G-quadruplex binding process and it is possible to obtain probes with high selectivity.

In addition, the detailed interactions of **1a** with G-quadruplex DNAs using various experiments and molecular docking were illustrated. **1a** exhibited sensitive fluorescence detection of G-quadruplex DNAs with the LOD values below  $1 \mu\text{M}$  in solution. Additionally, the CD experiments demonstrated that **1a** is able to sense G-quadruplex structures without affecting their topologies. Further studies showed that **1a** was inserted into the groove region of G-quadruplex structure and exhibited higher binding affinity to anti-parallel G-quadruplex structures. These results of this study gave some crucial factors on developing of effective probes for G-quadruplex DNA applications.

#### Acknowledgements

This work was financially supported by the General Program of Natural Science Foundation of the Higher Education Institutions of Jiangsu

Province (17KJB150009), the China Postdoctoral Science Foundation Funded Project (Grant No. 2017M611704).

#### Appendix A. Supplementary data

Supplementary data to this article can be found online at <https://doi.org/10.1016/j.saa.2018.03.083>.

#### References

- [1] M. Gellert, D.R. Davies, Proc. Natl. Acad. Sci. U. S. A. 48 (1962) 2013–2018.
- [2] S. Burge, G.N. Parkinson, P. Hazel, A.K. Todd, S. Neidle, Nucleic Acids Res. 34 (2006) 5402–5415.
- [3] H.J. Lipps, D. Rhodes, Trends Cell Biol. 19 (2009) 414–422.
- [4] P. Murat, S. Balasubramanian, Curr. Opin. Genet. Dev. 25 (2014) 22–29.
- [5] J.L. Huppert, FEBS J. 277 (2010) 3452–3458.
- [6] J.L. Huppert, S. Balasubramanian, Nucleic Acids Res. 33 (2005) 2908–2916.
- [7] S. Rankin, A.P. Reszka, J. Huppert, M. Zloh, G.N. Parkinson, A.K. Todd, S. Ladame, S. Balasubramanian, S. Neidle, J. Am. Chem. Soc. 127 (2005) 10584–10589.
- [8] D. Rhodes, H.J. Lipps, Nucleic Acids Res. 43 (2015) 8627–8637.
- [9] Q. Cao, Y. Li, E. Freisinger, P.Z. Qin, R.K.O. Sigel, Z.W. Mao, Inorg. Chem. Front. 4 (2017) 10–32.
- [10] G. Cimino-Reale, N. Zaffaroni, M. Folini, Curr. Pharm. Des. 22 (2016) 6612–6662.
- [11] T. Tian, H. Xiao, X. Zhou, Curr. Top. Med. Chem. 15 (2015) 1988–2001.
- [12] Z. Tan, J. Tang, Z.Y. Kan, Y.H. Hao, Curr. Top. Med. Chem. 15 (2015) 1940–1946.
- [13] T. Terai, T. Nagano, Pflugers Arch. - Eur. J. Physiol. 465 (2013) 347–359.
- [14] R. Balayeshwanth, V.J. Alzeer, N.W. Luedtke, Chembiochem 14 (2013) 540–558.
- [15] D.L. Ma, Z.H. Zhang, M.D. Wang, L.H. Lu, H.J. Zhong, C.H. Leung, Chem. Biol. 22 (2015) 812–828.
- [16] A.C. Bhasikuttan, J. Mohanty, Chem. Commun. 51 (2015) 7581–7597.
- [17] J. Mohanty, N. Barooah, V. Dhamodharan, S. Harikrishna, P.I. Pradeepkumar, A.C. Bhasikuttan, J. Am. Chem. Soc. 135 (2013) 367–376.
- [18] M. Zuffo, S. Ladame, F. Doria, M. Freccero, Sensors Actuators B Chem. 245 (2017) 780–788.
- [19] P. Yang, A.D. Cian, M.-P. Teulade-Fichou, J.-L. Mergny, D. Monchaud, Angew. Chem. Int. Ed. 48 (2009) 2188–2191.
- [20] M.-Q. Wang, Y. Wu, Z.-Y. Wang, Q.-Y. Chen, F.-Y. Xiao, Y.-C. Jiang, S. Amy, Dyes Pigments 145 (2017) 1–6.
- [21] Y.-J. Lu, X.-L. Guo, M.-H. Xu, W.-W. Chen, W.-L. Wong, K. Zhang, C.-F. Chow, Dyes Pigments 143 (2017) 331–341.
- [22] M.-H. Hu, S.-B. Chen, Y.-Q. Wang, Y.-M. Zeng, T.-M. Ou, D. Li, L.-Q. Gu, Z.-S. Huang, J.-H. Tan, Biosens. Bioelectron. 83 (2016) 77–84.
- [23] C.C. Chang, I.C. Kuo, I.F. Ling, C.T. Chen, H.C. Chen, P.J. Lou, J.J. Lin, T.C. Chang, Anal. Chem. 76 (2004) 4490–4494.
- [24] Y.-J. Lu, Q. Deng, J.-Q. Hou, D.-P. Hu, Z.-Y. Wang, K. Zhang, L.G. Luyt, W.L. Wong, C.F. Chow, ACS Chem. Biol. 11 (2016) 1019–1029.
- [25] Y. Wei, X. Zhang, L. Wang, Y. Liu, T. Bing, X. Liu, D. Shangguan, RSC Adv. 5 (2015) 75911–75917.
- [26] D. Lin, X. Fei, Y. Gu, C. Wang, Y. Tang, R. Li, J. Zhou, Analyst 140 (2015) 5772–5780.
- [27] F.H. Stootman, D.M. Fisher, A. Rodger, J.R. Aldrich-Wright, Analyst 131 (2006) 1145–1151.
- [28] O. Trott, A.J. Olson, J. Comput. Chem. 31 (2010) 455–461.
- [29] D. Sahoo, P. Bhattacharya, S. Chakravorti, J. Phys. Chem. B 114 (2010) 2044–2050.
- [30] C. Kumar, E.H. Asuncion, J. Am. Chem. Soc. 115 (1993) 8547–8553.
- [31] M. Shortreed, R. Kopelman, M. Kuhn, B. Hoyland, Anal. Chem. 68 (1996) 1414–1418.
- [32] N. Nagesh, V.K. Sharma, A.G. Kumar, E.A. Lewis, J. Nucleic Acids 2010 (2010) 146418.
- [33] Y. Hong, H. Xiong, J.W. Lam, M. Häußler, J. Liu, Y. Yu, Y. Zhong, H.H. Sung, I.D. Williams, K.S. Wong, B.Z. Tang, Chem. Eur. J. 16 (2010) 1232–1245.
- [34] B.T. Nguyen, E.V. Anslyn, Coord. Chem. Rev. 250 (2006) 3118–3127.
- [35] P.L.T. Tran, E. Laryg, F. Hamon, M.P. Teulade-Fichou, J.L. Mergny, Biochimie 93 (2011) 1288–1296.
- [36] Z.-Q. Liu, S.-T. Zhuo, J.-H. Tan, T.-M. Ou, D. Li, L.-Q. Gu, Z.-S. Huang, Tetrahedron 69 (2013) 4922–4932.
- [37] J. Li, D. Li, Y. Han, S. Shuang, C. Dong, Spectrochim. Acta A 73 (2009) 221–225.
- [38] J.R. Lakowicz, G. Webber, Biochemist 12 (1973) 4161–4170.